Rare Earth Engineering in RMn_6Sn_6 (R = Gd-Tm, Lu) Topological Kagome Magnets

Wenlong Ma,[1,*] Xitong Xu,[1,2,*] Jia-Xin Yin,[3,*] Hui Yang,[1] Huibin Zhou,[1] Zi-Jia Cheng,[3] Yuqing Huang,[1] Zhe Qu,[2,4] Fa Wang,[1,5] M. Zahid Hasan,[3,6,†] and Shuang Jia[1,5,7,8,‡]

[1]*International Center for Quantum Materials, School of Physics, Peking University, Beijing 100871, China*
[2]*Anhui Key Laboratory of Condensed Matter Physics at Extreme Conditions, High Magnetic Field Laboratory, HFIPS, Chinese Academy of Sciences, Hefei, Anhui 230031, China*
[3]*Laboratory for Topological Quantum Matter and Advanced Spectroscopy (B7), Department of Physics, Princeton University, Princeton, New Jersey 08544, USA*
[4]*CAS Key Laboratory of Photovoltaic and Energy Conservation Materials, Hefei Institutes of Physical Sciences, Chinese Academy of Sciences, Hefei, Anhui 230031, China*
[5]*Collaborative Innovation Center of Quantum Matter, Beijing 100871, China*
[6]*Materials Science Division, Lawrence Berkeley National Laboratory, Berkeley, California 94720, USA*
[7]*CAS Center for Excellence in Topological Quantum Computation, University of Chinese Academy of Sciences, Beijing 100190, China*
[8]*Beijing Academy of Quantum Information Sciences, West Building 3, No. 10 Xibeiwang East Road, Haidian District, Beijing 100193, China*

Exploration of the topological quantum materials with electron correlation is at the frontier of physics, as the strong interaction may give rise to new topological phases and transitions. Here we report that a family of kagome magnets RMn_6Sn_6 manifest the quantum transport properties analogical to those in the quantum-limit Chern magnet $TbMn_6Sn_6$. The topological transport in the family, including quantum oscillations with nontrivial Berry phase and large anomalous Hall effect arising from Berry curvature field, points to the existence of Chern gapped Dirac fermions. Our observation demonstrates a close relationship between rare-earth magnetism and topological electron structure, indicating the rare-earth elements can effectively engineer the Chern quantum phase in kagome magnets.

The interplay between lattice geometry and electron correlation can create new states of quantum matter [1–5], with recent examples including twisted bilayer graphene [6,7], Kitaev quantum spin liquid [8,9], and kagome Chern magnet [10,11]. A kagome lattice, consisting of two-dimensional corner-sharing triangles, naturally hosts both relativistic and dispersionless electrons [12,13], which are the origins of its nontrivial band topology. With the inclusion of magnetism and spin-orbit coupling (SOC), kagome electrons can realize strongly interacting topological phases [10,12,14]. Recent study [11] has found a near-ideal quantum limit Chern magnet $TbMn_6Sn_6$, which hosts defect-free Mn kagome lattice. However the topological nature of other members in the RMn_6Sn_6 (R = rare-earth element) family remains largely unexplored. The RMn_6Sn_6 system features a pristine Mn_3 kagome lattice [Fig. 1(a)] in a layered structure [15]. They all exhibit magnetic ordering of Mn moments at room temperature while different R gives rise to various magnetic structures [16–18]. Of particular interest, $TbMn_6Sn_6$ manifests a ferrimagnetic (FIM) structure in which Tb sublattice is antiparallel with out-of-plane ferromagnetically (FM) ordered Mn lattice. This FIM structure has been proven to effectively sustain the spinless Haldane model generating Chern gapped massive Dirac fermions (MDFs), as illustrated in Fig. 1(b) [4,10,11].

In this work we investigate the topological properties of the Mn kagome lattices in a series of RMn_6Sn_6 (R = Gd–Tm, Lu). Their magnetic ground states are classified as FIM when R = Gd to Ho, and antiferromagnetic (AFM) when R is Er, Tm, and Lu [15] [Fig. 1(c)]. We found in general MDFs exist in the FM ordered kagome lattice of RMn_6Sn_6 but is absent in the AFM states. The Chern gap (Δ) and the Dirac cone energy (E_D) follow a decreasing trend from R = Gd to Er. As we argue below, this R engineering on the topological electron structure is intimately related to the coupling between $4f$ local moment and Mn $3d$ moment. In particular, Δ is proportional to the de Gennes factor (dG) of $4f$ moments while E_D is proportional to $\sqrt{\mathrm{dG}}$. The interplay of the magnetic order and topological structure remains a fertile ground in the systems with strong correlation. Our finding demonstrates that a local-moment-bearing R can serve as a knob for tuning the topological properties in quantum magnets.

RMn_6Sn_6 single crystals were synthesized via a flux method [18,21]. All these metals are magnetically ordered above room temperature [Fig. 1(e)] while the magnetic R

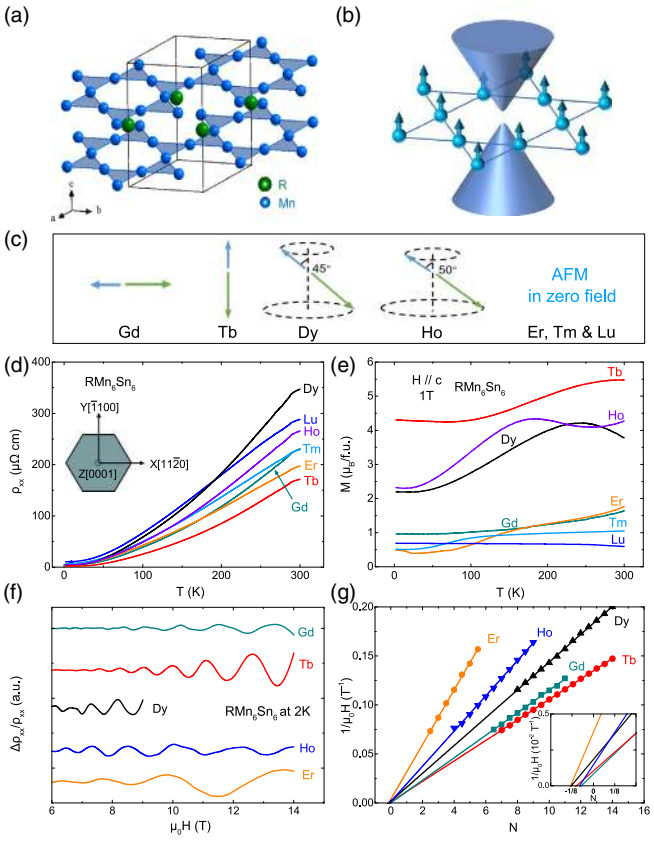

FIG. 1. Crystal structure, physical property, and topological electrons in $R\mathrm{Mn_6Sn_6}$. (a) Mn kagome layers and R sublattices in $R\mathrm{Mn_6Sn_6}$. (b) Illustration of MDF with a Chern gap in the magnetic kagome lattice. (c) Magnetic structures in zero field. Blue and green arrows represent the direction of Mn and R moments, respectively. (d) $\rho(T)$ curves for single crystals. Inset: crystallographic orientations. (e) $M(T)$ for $\mu_0 H = 1$ T. (f) SdH QOs at 2 K. (g) Landau fan diagram. Peak positions in (f) are assigned with half-integral Landau indexes [19,20]. Inset: closeup near $N = 0$.

sublattice tends to develop an antiparallel configuration with respect to Mn if the Mn lattice is FM ordered [17,18]. The magnetic anisotropy varies from easy ab plane for $R = \mathrm{Gd}$, to easy c axis for $R = \mathrm{Tb}$, and to a conical magnetic structure for $R = \mathrm{Dy}$ and Ho [16–18]. When R is Er and Tm, the Mn and Er/Tm sublattices are independently ordered in an AFM manner because the strength of the magnetic coupling is weak [17,18]. As there is no $4f$ moment in $\mathrm{LuMn_6Sn_6}$, its magnetic structure was reported to be a flat spiral AFM [22], similar to that in $\mathrm{YMn_6Sn_6}$ [23–25].

One remarkable feature is that those demonstrating FIM order ($R = \mathrm{Gd}$ to Er) all exhibit Shubnikov-de Haas quantum oscillations (SdH QOs) with a close and small oscillatory frequency [Fig. 1(f)]. We obtain the Berry phases according to the Lifshitz-Onsager quantization rule [26], $F/B_N + \gamma = N$, where F is the oscillatory frequency, B_N is the Nth minimum in ρ_{xx}, $\gamma = 1/2 - \beta$, and β is the Berry phase. The intercepts on the N-index axis in Fig. 1(g) all give γ close to $-1/8$, pointing to a same nontrivial Berry phase [19,20,27]. Corresponding cyclotron mass m^* is estimated to be around $0.1m_e$ by fitting to the Lifshitz-Kosevich formula [26] (see Table I, Sec. VI of the Supplemental Material [28]). The Fermi velocity ($v_F \simeq \sqrt{2e\hbar F}/m^*$) is found to be around 5×10^5 m/s.

The above analyses demonstrate that the electronic structures of $R\mathrm{Mn_6Sn_6}$ resemble each other, which is expected as their lattice parameters differ less than 0.4%. A series of experiments including the scanning tunneling microscopy (STM) and angle-resolved photoemission spectroscopy (ARPES) [11] connect the SdH QOs with the MDF in $\mathrm{TbMn_6Sn_6}$. This connection is also experimentally established in $\mathrm{GdMn_6Sn_6}$ (ARPES data in Sec. II of the Supplemental Material [28]). We conclude that the Chern gapped MDF is generally hosted in FM Mn kagome lattice of $R\mathrm{Mn_6Sn_6}$ ($R = \mathrm{Gd}$ to Er). We highlight two key features of these QOs that constrain our analysis along this direction. First, the Fermi surface of the pocket is detected to be 2D in angular dependent measurements [11]. Second, the QOs are intimately related with the FM order in the Mn kagome lattice ($R = \mathrm{Gd}$ to Ho and Er) while no QO is observed in AFM Tm, Lu, or Y members.

To further understand the interplay between the magnetic structure and topological property, we systematically study the magnetization and anomalous Hall effect as shown in Fig. 2. We take $\mathrm{DyMn_6Sn_6}$ as an example, which has a conical magnetic structure below room temperature. The $M(H)$ shows a hard-magnetlike profile with sharp, considerable hysteresis loops below 100 K [Fig. 2(c)]. With increasing external field, there exists a continuous rotation of the magnetic moments towards the c axis. The Hall resistivity (ρ_{yx}) resembles the profile of its $M(H)$ completely. We separate the anomalous contribution (Sec. III of the Supplemental Material [28]) using the empirical relation [37],

$$\rho_{yx} = \rho_{\mathrm{OH}}(B) + \rho_{\mathrm{AH}}(M) = R_0 B + R_S 4\pi M \qquad (1)$$

where ρ_{OH} and ρ_{AH} represent ordinary and anomalous Hall resistivity, R_0 and R_S are ordinary and anomalous Hall coefficients, respectively. Similar phenomena hold for Gd,

TABLE I. MDFs in $R\mathrm{Mn_6Sn_6}$. σ^{int}: the intrinsic anomalous Hall conductivity. F and m^*: frequency and cyclotron mass of SdH QOs. v_F and k_F: Fermi velocity and wave vector.

R	σ^{int} (e^2/h)	$F(T)$	m^* (m_e)	v_F (10^5 m/s)	k_F (Å^{-1})
Gd	0.14	87	0.11	5.4	0.051
Tb	0.12	96	0.14	4.5	0.054
Dy	0.06	71	0.10	5.4	0.046
Ho	0.09	55	0.12	4.0	0.041
Er	0.04	35	0.11	3.4	0.033

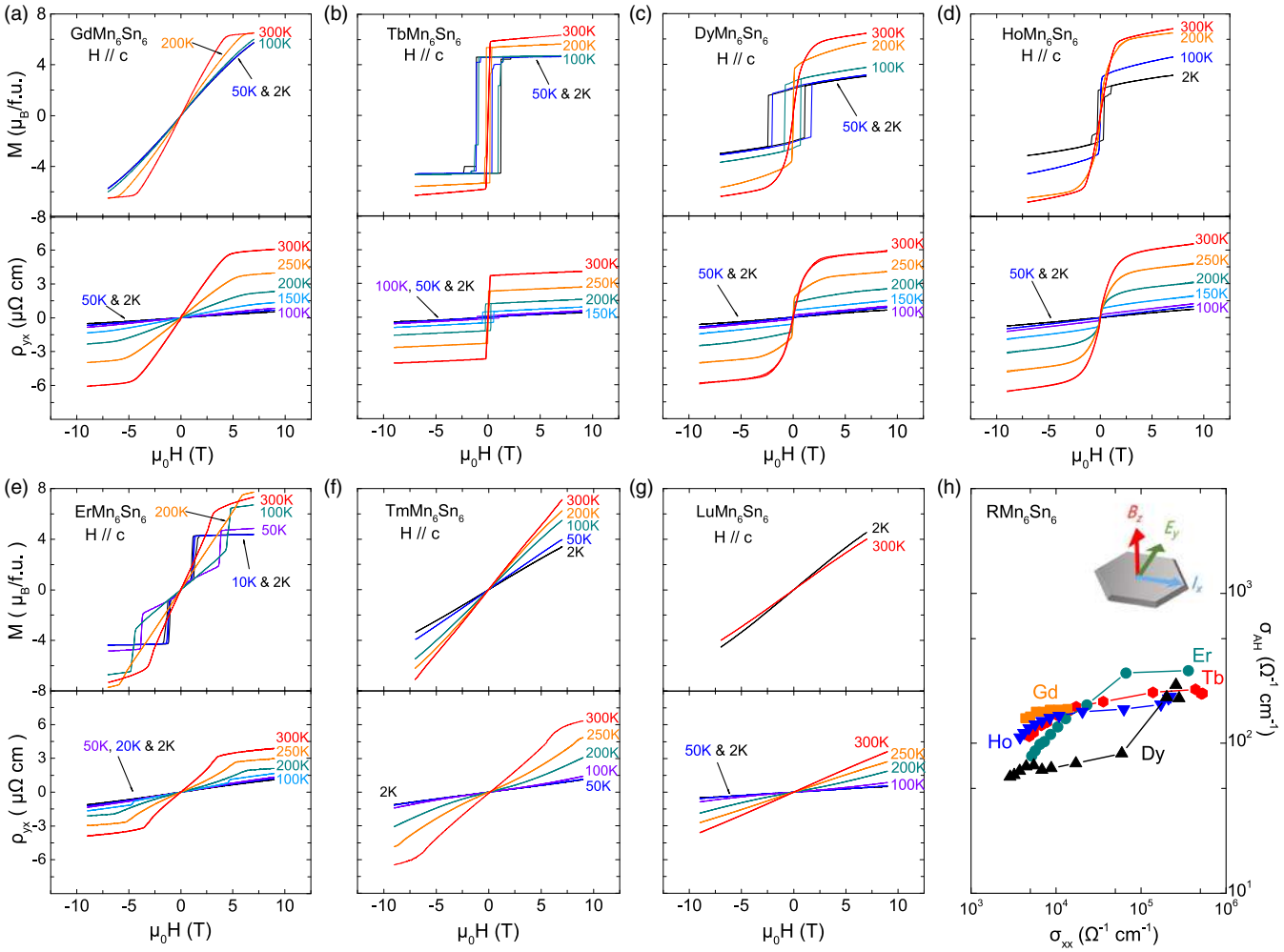

FIG. 2. (a)–(g): Magnetization and Hall resistivity of RM_6Sn_6. (h) Anomalous Hall conductivity σ_{AH} versus σ_{xx}. Inset: Hall measurement configuration.

Tb, and Ho members. $ErMn_6Sn_6$ lies between FIM and AFM states and a small field triggers a metamagnetic transition which represents a sharp jump on the $M(H)$ curves below 100 K [Fig. 2(e)] [15,18]. Its ρ_{yx} curves also follow the $M(H)$ curves [Fig. S5(e)] and we can distinguish $\rho_{\rm AH}$ as the step on the transition. For Tm and Lu, the stable AFM structure [17,18] defies explicit zero-field anomalous effect in their ρ_{yx}, similar as the observation for YMn_6Sn_6 [23,24]. Interestingly, $\rho_{\rm AH}$ in $TmMn_6Sn_6$ deviates from the linear $M(H)$ above 100 K [Fig. 2(f)], which might arise from a topological Hall effect (THE) and deserves attention in the future.

The scaling relation between the anomalous Hall conductivity (AHC) $\sigma_{\rm AH} \simeq \rho_{\rm AH}/\rho_{xx}^2$ and σ_{xx} is shown in Fig. 2(h). Previous studies have identified three distinct regimes which are delimited by σ_{xx} and characterized by the dependence of $\sigma_{\rm AH}$ and σ_{xx} [37–40]. For RMn_6Sn_6, σ_{xx} ranges from 3×10^3 to $5\times10^5\ \Omega^{-1}\,{\rm cm}^{-1}$, approximately lying within the good-metal regime. Their $\sigma_{\rm AH}$, of the order $100\ \Omega^{-1}\,{\rm cm}^{-1}$, keeps nearly invariant in this regime, suggesting dominant intrinsic contributions. By fitting the scaling law (Sec. V of the Supplemental Material [28]), we extract the intrinsic Hall conductivity $\sigma^{\rm int}$ to be around $0.14-0.04e^2/h$ per kagome layer for $R=$ Gd to Er, as summarized in Table I.

A high-temperature quantum anomalous Hall effect with a quantized Hall value e^2/h is theoretically supported by a Chern insulating gap of the MDF [10]. In RMn_6Sn_6, the Chern gap is near the Fermi level and therefore its Berry curvature field should induce a large intrinsic AHC. The AHC for MDF is estimated as [41]

$$\sigma^{\rm int} = \frac{e^2}{h}\frac{\Delta}{\sqrt{\Delta^2+4\hbar^2k_F^2v_F^2}} = \frac{e^2}{h}\frac{\Delta/2}{E_D}. \qquad (2)$$

As Δ and E_D in $TbMn_6Sn_6$ have been completed depicted by STM, the agreement between theoretically inferred AHC and our transport data indicates that the MDF dominates the Berry curvature field [11]. Assuming $\sigma^{\rm int}$ is stemming from the MDF in the kagome lattice in other

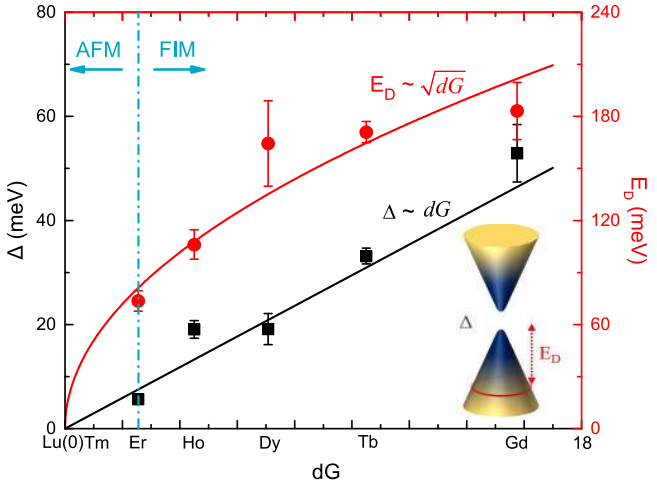

FIG. 3. Derived Dirac cone energy E_D and gap size Δ for the whole series. The systematic evolution of E_D and Δ follows $\sqrt{\mathrm{dG}}$ and dG, respectively. Inset: sketch of a Chern gapped Dirac cone.

$R\mathrm{Mn_6Sn_6}$ as well, we evaluate the effective Δ and E_D. Interestingly, both parameters gradually decrease when R changes from Gd to Er (Fig. 3).

The analysis highlights the possibility of Chern phase engineering in $R\mathrm{Mn_6Sn_6}$ by changing the R atoms. Regulating the Chern gap has been less accomplished in experiments and one example is Fe_3Sn_2 whose gap can be modulated by applying an external magnetic field [42,43]. Here we observe a unique, intrinsic R engineering of topological electrons in a kagome magnet, and its mechanism needs further elaboration. The chemical pressure does not likely play a role because the lattice parameter changes little in the series. On the other hand, the total SOC strength should increase slightly with the atomic number from R = Gd to Er, which is opposite the trend of gap closing. Below we discuss one possible mechanism.

When we plot Δ and E_D against $\mathrm{dG} = (g_J - 1)^2 J(J+1)$, where g_J is the Landé factor and J is the total angular momentum of the R^{3+} ion Hund's rule ground state, we find they apparently follow a linear and square root relation, respectively, as shown in Fig. 3. We propose that the coupling between $4f$ moments and $3d$ electrons of Mn plays a crucial role in this engineering. If we include the hopping between Mn and R [Fig. 4(a)], it will introduce an additional diagonal component in total Hamiltonian, which is proportional to $-J_H m$, where J_H is the Hund's coupling, and $m = (g_J - 1)\sqrt{J(J+1)} = \sqrt{\mathrm{dG}}$ is the effective moment of R ions in mean-field approximation [44]. Considering this first-order hopping process, we naturally conclude that the chemical potential of the MDF should shift linearly with $\sqrt{\mathrm{dG}}$. The first-order process should not contribute to the gap opening on the $K(K')$ valley because of the symmetry of a kagome lattice. To elucidate the gap opening, a higher order process [for instance, the two-electron hopping in Fig. 4(b)] has to be

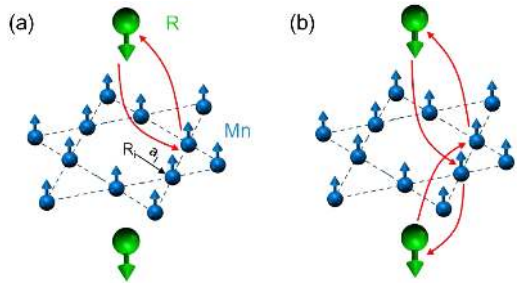

FIG. 4. Sketch of possible electron hopping between R and Mn kagome in FIM $R\mathrm{Mn_6Sn_6}$. (a) First-order process involving one-electron hopping. (b) Second-order process involving two-electron hopping.

considered (Sec. VII of the Supplemental Material [28]). The forth-order perturbation will open a gap proportional to $\sim J_H^2 m^2$, namely $\Delta \propto \mathrm{dG}$, just as what we have observed in experiment.

The magnetic exchange coupling between $3d$ and $4f$ electrons plays an important role in the magnetic properties of $R\mathrm{Mn_6Sn_6}$ as well [15–18]. Phenomenologically, this coupling is weakened when R changes from Gd to Tm. $\mathrm{ErMn_6Sn_6}$ has a critically weak coupling which makes it lie at the border between FIM and AFM ground states and we notice it also has the smallest Δ and E_D. This interesting observation supports the critical role of magnetic coupling in the MDF structure. On the other hand, the THE and electronic structure in $\mathrm{YMn_6Sn_6}$ which has no $4f$ moments, deserve further elaboration [23–25]. Our work highlights the material system which not only largely extends the family of quantum kagome magnets but also intrinsically contains a quantum knob for Chern phase engineering. The quantum tuning of the topological band structures via magnetic coupling may serve as a pathway to engineer the topological phases in correlated systems.

We thank Weiwei Xie for helpful discussions about the crystal structure and Jingzhuo Zhou for assistance in figure drawing. Z. C. thanks D. Lu and M. Hashimoto at Beamline 5-2 of the Stanford Synchrotron Radiation Lightsource (SSRL) at the SLAC National Accelerator Laboratory, CA, USA for support. This work was supported by the National Natural Science Foundation of China Grants No. U1832214, No. 11774007, No. U2032213, No. 11774352, the National Key R&D Program of China (2018YFA0305601), and the strategic Priority Research Program of Chinese Academy of Sciences, Grant No. XDB28000000. X. X. acknowledges support from the China Postdoctoral Science Foundation Grant No. 2020M682056, Anhui Postdoctoral Foundation Grant No. 2020B472, the HFIPS Director's Fund Grant No. YZJJ2021QN28, and Special Research Assistant Program, Chinese Academy of Sciences. Experimental and theoretical work at Princeton University was supported by the Gordon and Betty Moore Foundation (Grants

No. GBMF4547 and No. GBMF9461/Hasan). Work at Princeton University and Princeton-led synchrotron-based ARPES measurements are supported by the U.S. Department of Energy under Grant No. DOE/BES DE-FG-02-05ER46200. Use of the Stanford Synchrotron Radiation Lightsource (SSRL), SLAC National Accelerator Laboratory, is supported by the U.S. Department of Energy, Office of Science, Office of Basic Energy Sciences, under contract No. DE-AC02-76SF00515.

*These authors contributed equally to this work.
†mzhasan@princeton.edu
‡gwljiashuang@pku.edu.cn

[1] B. Keimer and J. Moore, Nat. Phys. **13**, 1045 (2017).
[2] S. Sachdev, Rep. Prog. Phys. **82**, 014001 (2019).
[3] P. C. Canfield, Rep. Prog. Phys. **83**, 016501 (2020).
[4] F. D. M. Haldane, Phys. Rev. Lett. **61**, 2015 (1988).
[5] C.-Z. Chang, J. Zhang, X. Feng, J. Shen, Z. Zhang, M. Guo, K. Li, Y. Ou, P. Wei, L.-L. Wang *et al.*, Science **340**, 167 (2013).
[6] R. Bistritzer and A. H. MacDonald, Proc. Natl. Acad. Sci. U.S.A. **108**, 12233 (2011).
[7] Y. Cao, V. Fatemi, A. Demir, S. Fang, S. L. Tomarken, J. Y. Luo, J. D. Sanchez-Yamagishi, K. Watanabe, T. Taniguchi, E. Kaxiras *et al.*, Nature (London) **556**, 80 (2018).
[8] A. Kitaev, Ann. Phys. (Amsterdam) **321**, 2 (2006), January Special Issue.
[9] Y. Kasahara, T. Ohnishi, Y. Mizukami, O. Tanaka, S. Ma, K. Sugii, N. Kurita, H. Tanaka, J. Nasu, Y. Motome *et al.*, Nature (London) **559**, 227 (2018).
[10] G. Xu, B. Lian, and S.-C. Zhang, Phys. Rev. Lett. **115**, 186802 (2015).
[11] J.-X. Yin, W. Ma, T. A. Cochran, X. Xu, S. S. Zhang, H.-J. Tien, N. Shumiya, G. Cheng, K. Jiang, B. Lian *et al.*, Nature (London) **583**, 533 (2020).
[12] K. Ohgushi, S. Murakami, and N. Nagaosa, Phys. Rev. B **62**, R6065 (2000).
[13] Z.-Y. Zhang, J. Phys. Condens. Matter **23**, 365801 (2011).
[14] E. Tang, J.-W. Mei, and X.-G. Wen, Phys. Rev. Lett. **106**, 236802 (2011).
[15] L. Zhang, *Unusual Magnetic Behavior of Some Rare-Earth and Manganese Compounds* (Enschede: Printerpartners Ipskamp B.V., Enschede, 2005).
[16] G. Venturini, B. E. Idrissi, and B. Malaman, J. Magn. Magn. Mater. **94**, 35 (1991).
[17] B. Malaman, G. Venturini, R. Welter, J. Sanchez, P. Vulliet, and E. Ressouche, J. Magn. Magn. Mater. **202**, 519 (1999).
[18] D. Clatterbuck and K. Gschneidner, J. Magn. Magn. Mater. **207**, 78 (1999).
[19] C. M. Wang, H.-Z. Lu, and S.-Q. Shen, Phys. Rev. Lett. **117**, 077201 (2016).
[20] H. Murakawa, M. Bahramy, M. Tokunaga, Y. Kohama, C. Bell, Y. Kaneko, N. Nagaosa, H. Hwang, and Y. Tokura, Science **342**, 1490 (2013).
[21] P. C. Canfield and Z. Fisk, Philos. Mag. B **65**, 1117 (1992).
[22] G. Venturini, R. Welter, B. Malaman, and E. Ressouche, J. Alloys Compd. **200**, 51 (1993).
[23] N. J. Ghimire, R. L. Dally, L. Poudel, D. Jones, D. Michel, N. T. Magar, M. Bleuel, M. A. McGuire, J. Jiang, J. Mitchell *et al.*, Sci. Adv. **6**, eabe2680 (2020).
[24] Q. Wang, K. J. Neubauer, C. Duan, Q. Yin, S. Fujitsu, H. Hosono, F. Ye, R. Zhang, S. Chi, K. Krycka, H. Lei, and P. Dai, Phys. Rev. B **103**, 014416 (2021).
[25] M. Li, Q. Wang, G. Wang, Z. Yuan, W. Song, R. Lou, Z. Liu, Y. Huang, Z. Liu, H. Lei *et al.*, Research Square preprint (2020), https://doi.org/10.21203/rs.3.rs-114140/v1.
[26] D. Shoenberg, *Magnetic Oscillations in Metals* (Cambridge University Press, Cambridge, England, 2009).
[27] G. P. Mikitik and Y. V. Sharlai, Phys. Rev. B **85**, 033301 (2012).
[28] See Supplemental Material at http://link.aps.org/supplemental/10.1103/PhysRevLett.126.246602, which includes Refs. [29–36], for experimental and theoretical details as well as additional figures and discussions.
[29] L. Ye, M. Kang, J. Liu, F. Von Cube, C. R. Wicker, T. Suzuki, C. Jozwiak, A. Bostwick, E. Rotenberg, D. C. Bell *et al.*, Nature (London) **555**, 638 (2018).
[30] Q. Wang, Y. Xu, R. Lou, Z. Liu, M. Li, Y. Huang, D. Shen, H. Weng, S. Wang, and H. Lei, Nat. Commun. **9**, 3681 (2018).
[31] C. Hurd, *The Hall Effect in Metals and Alloys* (Springer Science & Business Media, Berlin, 2012).
[32] C. Zeng, Y. Yao, Q. Niu, and H. H. Weitering, Phys. Rev. Lett. **96**, 037204 (2006).
[33] Y. Tian, L. Ye, and X. Jin, Phys. Rev. Lett. **103**, 087206 (2009).
[34] M. N. Ali, J. Xiong, S. Flynn, J. Tao, Q. D. Gibson, L. M. Schoop, T. Liang, N. Haldolaarachchige, M. Hirschberger, N. Ong *et al.*, Nature (London) **514**, 205 (2014).
[35] A. A. Abrikosov, Phys. Rev. B **58**, 2788 (1998).
[36] A. A. Abrikosov, Europhys. Lett. **49**, 789 (2000).
[37] N. Nagaosa, J. Sinova, S. Onoda, A. H. MacDonald, and N. P. Ong, Rev. Mod. Phys. **82**, 1539 (2010).
[38] S. Onoda, N. Sugimoto, and N. Nagaosa, Phys. Rev. Lett. **97**, 126602 (2006).
[39] T. Miyasato, N. Abe, T. Fujii, A. Asamitsu, S. Onoda, Y. Onose, N. Nagaosa, and Y. Tokura, Phys. Rev. Lett. **99**, 086602 (2007).
[40] S. Onoda, N. Sugimoto, and N. Nagaosa, Phys. Rev. B **77**, 165103 (2008).
[41] N. A. Sinitsyn, A. H. MacDonald, T. Jungwirth, V. K. Dugaev, and J. Sinova, Phys. Rev. B **75**, 045315 (2007).
[42] J.-X. Yin, S. S. Zhang, H. Li, K. Jiang, G. Chang, B. Zhang, B. Lian, C. Xiang, I. Belopolski, H. Zheng *et al.*, Nature (London) **562**, 91 (2018).
[43] L. Ye, M. K. Chan, R. D. McDonald, D. Graf, M. Kang, J. Liu, T. Suzuki, R. Comin, L. Fu, and J. G. Checkelsky, Nat. Commun. **10**, 4870 (2019).
[44] J. Jensen and A. R. Mackintosh, *Rare Earth Magnetism* (Clarendon Press, Oxford, 1991).